JMEPEG (2015) 24:209–220
DOI: 10.1007/s11665-014-1254-7

1059-9495/$19.00

High Temperature Formability Prediction of Dual Phase Brass Using Phenomenological and Physical Constitutive Models

E. Farabi, A. Zarei-Hanzaki, and H.R. Abedi

(Submitted July 17, 2014; in revised form September 15, 2014; published online October 17, 2014)

Characterizing the high temperature flow behavior of a lead bearing duplex brass in a wide range of forming temperatures (673-1073 K) and strain rates (0.001-0.1 s^{-1}) has been conducted in the present work. In order to establish the constitutive equations, two major modeling procedures, phenomenological (the Original Johnson-Cook and the Arrhenius-type) and physically based (the modified Zerilli-Armstrong) models, have been employed. The capability and accuracy of each model has been assessed via standard statistical parameters such as average absolute relative error and correlation coefficient. The comparative and comprehensive study of the flow behavior indicated that the accuracy of the phenomenological models was strongly dependent on the range of the testing temperatures and the corresponding mechanism which operate under the specified deformation conditions. It has been indicated that by limiting the temperature range a more precise *Q*-value is reached, which positively influences the accuracy of the Arrhenius-type model. In contrast, the modified Zerilli-Armstrong model was capable to overcome these limitations and properly considers the physical characteristics including dislocation dynamics and thermal activation to develop the materials constants.

Keywords constitutive equations, flow behavior, formability, high temperature deformation

1. Introduction

The widespread and ongoing popularity of copper-zinc alloys (i.e., brasses), is the ease with which they are being processed to finished and semi-finished products, such as rods, profiles, or sheets (Ref 1). Conventionally, they are thermomechanically processed (TMP) at high temperatures, where the material experiences a complex combination of strain, strain rate and temperature (Ref 2). To this end, achieving the desired mechanical properties is in dependent on how suitable thermomechanical processing (TMP) routes are designed. The latter is achieved by proper understanding of the material's response to external loadings. In this regard, constitutive modeling is used as a powerful tool for predicting the material behavior under specified deformation conditions (Ref 3-5).

Up to date, many constitutive relationships including phenomenological and physical-based models have been presented to predict the high temperature flow behavior of the materials. Phenomenological constitutive models provide a definition of the flow stress based on the empirical observations, and consist of some mathematical functions (Ref 6, 7) In this regard, the Johnson-Cook (JC) constitutive model (Ref 8) has been successfully incorporated in finite element analyzing packages to describe the variation of the flow stress with forming temperature, strain rate and imposed strain, in a simple multiplication form (Ref 9). Lin et al. have recently utilized the original Johnson-cook model to predict the flow stress of the Al-Mg-Cu alloy (Ref 10). They proposed this model as an accurate constitutive equation to estimate the high temperature loading responses of the corresponding alloy. In another approach the hyperbolic sine Arrhenius-type constitutive equation as a phenomenological model has been successfully applied to predict the elevated temperature flow behavior of the materials. This model was proposed by Sellars and MacTegart (Ref 11) where the flow stress would be expressed by the sine-hyperbolic law in an Arrhenius-type of equation. The original model has been revised several times to suitably represent the elevated temperature response of various alloys to the external loadings. Sloof et al. (Ref 12) have introduced a strain-dependent parameter into the hyperbolic constitutive equation in order to improve the capability of the proposed model. This approach has been employed by various researchers, and the constitutive behaviors of pure titanium (Ref 13), 42CrMo steel (Ref 14), Ti-modified austenitic stainless steel (Ref 15), Ni-Ti shape memory alloy (Ref 16), copper (Ref 17), and copper alloys (Ref 18) have been formulated.

In contrast to previous phenomenological flow stress models, a modified Zerilli-Armstrong model was proposed by Samantaray et al. (Ref 19). This has been successfully employed to describe the high temperature flow behavior of ferrous (Ref 16) and non-ferrous materials (Ref 20). Apparently, the physical characteristics including dislocation dynamics and thermal activation are employed as the main features to develop the materials constants. The Zerilli-Armstrong model

E. Farabi, A. Zarei-Hanzaki, and **H. R. Abedi**, The Complex Laboratory of Hot Deformation & Thermomechanical Processing of High Performance Engineering Materials, School of Metallurgy and Materials Engineering, College of Engineering, University of Tehran, Tehran, Iran. Contact e-mail: zareih@ut.ac.ir.

(Ref 21) and its modified form considers the effects of thermal softening, strain rate hardening, and isotropic hardening as well as the coupled effects of temperature, strain, and strain rate on the flow stress. The capability of this model has been assessed in the case of 20CrMo steel (Ref 22), modified 9Cr-1Mo steel (Ref 23), Ti-6Al-4V (Ref 21), and 7050 aluminum alloy (Ref 20).

The high temperature deformation behavior of metallic materials has been always accompanied with various interconnecting metallurgical phenomena such as work hardening, dynamic recovery, dynamic recrystallization, and flow instability. Consequently, the modeling and prediction of high temperature flow behavior of metallic materials is quite complex in nature and each constitutive model holds its own drawbacks and errors in predicting the behavior of the material at elevated temperatures. In this aspect many researchers have investigated the capability of each model for various materials in different range of temperatures and strain rates (Ref 24-26). In line to previous efforts, the objective of this investigation is to establish the constitutive equations based on phenomenological (original Johnson-Cook and strain-compensated Arrhenius-type) and physically based models (modified Zerilli-Armstrong), and make a comparative study on their capability to predict the elevated temperature flow behavior of a leaded duplex brass in a wide range of temperatures and strain rates. The suitability of these three models has been evaluated by comparing the correlation coefficient and average absolute relative error (AARE) of prediction, the ability to track the deformation behavior, and the numbers of material constants.

2. Experimental Procedure

A leaded duplex brass in as-extruded condition holding the chemical composition given in Table 1 was considered as experimental material. The initial microstructure of the as-received material is given in Fig. 1. The presence of coarse alpha grains elongated in parallel to the extrusion direction, beta phase matrix and annealing twins inside the alpha grains are clearly evident through the microstructure. The hot compression cylindrical specimens were prepared in accordance with ASTM E209 standard (8 mm in diameter × 12 mm in height). The hot compression tests were carried out using a Gotech AI-700 LA 30 servo controlled electronic universal testing machine equipped with an electrical resistance furnace. The corresponding thermomechanical processing (TMP) cycles were performed in the temperature range of 673 to 1073 K under the strain rates of 0.001, 0.01, and 0.1 s^{-1}. The reduction in height was programed to be 60% by the end of the compression tests. Prior to any hot compression test, the specimens were first preheated to the preset temperature in an electric resistant furnace and soaked for 5 min. to equilibrate the temperature throughout the specimens. The specimens were immediately quenched in water right at the end of straining. The true stress values were recorded using a high accurate load cell (Model: SSMDJM- 20kN) affording the capability of measuring the load forces down to 0.1 kg. The displacement data were used to compute the true strain values. A very thin mica plate was used to minimize the friction effects. Each cycle was repeated three times in order to maintain the reliability of the experimental procedure and the mean flow stress was reported.

Table 1 Chemical composition of the experimental leaded duplex brass (wt.%)

Cu	Fe	Pb	Sb	Bi	Zn
58.50	<0.15	1.5	<0.005	<0.002	Bal.

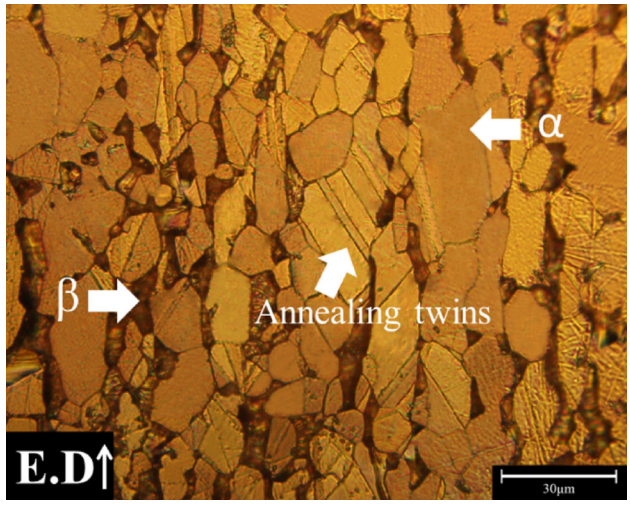

Fig. 1 Initial microstructure of the experimental alloy

3. Results and Discussions

The typical true stress- true strain curves obtained in different thermomechanical conditions are represented in Fig. 2. To justify the effect of friction, the flow behavior has been corrected and the corresponding curves are also superimposed on each curve (Ref 27). According to the previous researches (Ref 28, 29), some methods to evaluate the average friction coefficient in bulk metal forming have been proposed for cylindrical specimens; a typical formulation is given by

$$\mu = \frac{\frac{R}{h} \times b}{\frac{4}{\sqrt{3}} - \frac{2b}{3\sqrt{3}}}, \quad \text{(Eq 1)}$$

where μ is the average friction coefficient of the entire working process varying from 0 (perfect sliding) to 1 (sticking), b is the barreling factor, and R and h are the theoretical radius and final height of the sample respectively; b is given by (Ref 28, 29)

$$b = 4\frac{\Delta R}{R} \times \frac{h}{\Delta h}. \quad \text{(Eq 2)}$$

As it is illustrated in Fig. 3, ΔR and Δh are the differences between the maximum radius (R_m) and the top radius (R_t) of the sample and the reduction in height for the cylinder after compression, respectively. To eliminate the friction effect from the deformation curve, the following equation can be used (Ref 28-30):

$$\sigma = \frac{C^2 P}{2[\exp(C) - C - 1]}, \quad \text{(Eq 3)}$$

where $C = \frac{2\mu r}{h}$, and r and h are the original radius and the height of the sample. μ is a constant obtained from Eq 1 and

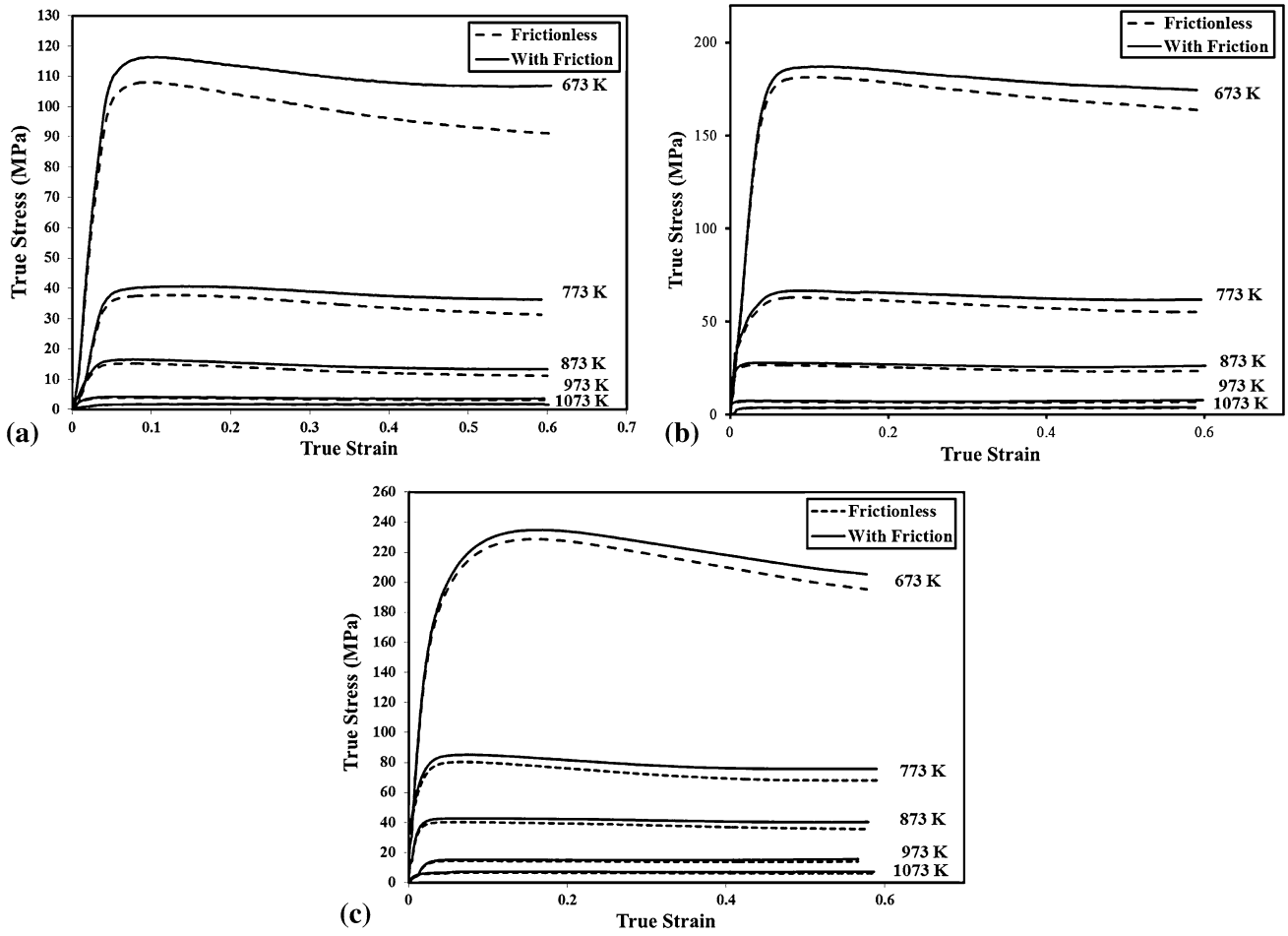

Fig. 2 Comparison between the corrected and measured true sress-true strain curves at different temperature under strain rates of: (a) 0.001 s^{-1}, (b) 0.01 s^{-1}, (c) 0.1 s^{-1}

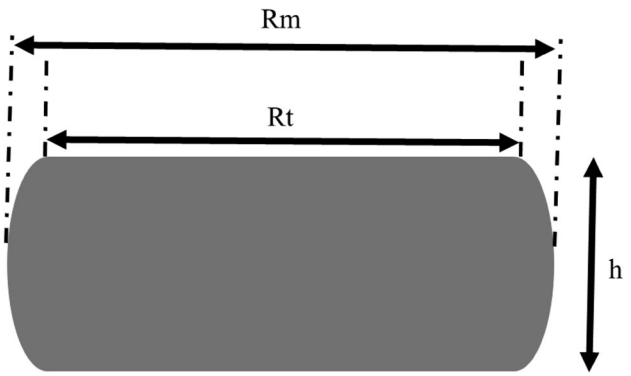

Fig. 3 Schematic figure of the specimen shape change after hot compression process

P is the experimental true stress of the specimen. Therefore, by combining Eqs 1 and 3, the correction of true stress-true strain curves can be done.

According to the obtained flow curves (Fig. 2), it can be easily found that the corrected flow stresses generally are lower than the measured ones, which reflects the negative effects of interfacial friction on the flow stress. In addition, the flow behavior is significantly affected by the deformation temperature and strain rate. These figures reveal the typical recrystallization-accompanied plastic flow (Ref 31, 32), where a single peak is followed by work softening down to the steady state regime at higher imposed strain. These findings are in accordance with previous reported results trying to characterize the recrystallization behavior of duplex brass from the qualitative point of view (Ref 33). Interestingly, a sharp transition in stress level is realized by increasing deformation temperature from 673 to 773 K. As is well established (Ref 2), this can be justified considering the occurrence of order-disorder transformation at about 727-736 K. As a matter of fact, the strengthening effect of ordered β′ phase (B2 structure) will be lost due to the occurrence of this diffusional transformation. These will be properly employed to assess the high temperature flow behavior of the alloy from the quantitative viewpoint.

3.1 Constitutive Modeling

3.1.1 The Original Johnson-Cook (JC) Model. The original Johnson-Cook model (Ref 8), which has been successfully employed for a variety of materials in a wide range of deforming temperatures and strain rates (Ref 26) is expressed as

$$\sigma = (A + B\varepsilon^{n})\left[1 + C\ln\left(\frac{\dot{\varepsilon}}{\dot{\varepsilon}_0}\right)\right](1 - T^{*p}), \qquad \text{(Eq 4)}$$

where σ is the equivalent flow stress, A is the yield stress at reference temperature and reference strain rate, ε is the

equivalent plastic strain, n is the exponent of strain hardening, and B is the strain hardening coefficient. C and p are the material constants that represent the coefficient of strain-rate hardening and the thermal softening exponent, respectively. $\dot{\varepsilon}$ is the strain rate, while $\dot{\varepsilon}_0$ is the reference strain rate, and T^* is the homologous temperature, which is expressed as $T^* = (T - T_r)/(T_m - T_r)$; T is the absolute temperature, T_m is the melting temperature (1175 K for the experimental alloy), and T_r is the reference temperature. The lowest test temperature (673 K) and strain rate (0.001 s^{-1}) are chosen as the reference temperature (T_r) and the reference strain rate ($\dot{\varepsilon}$), respectively; these would ensure a successful calculation of material constants. The yield stress (A) at reference temperature and reference strain rate is measured to be 98 Mpa. The Eq 4 can be simplified as is follows where the strain rate is 0.001 s^{-1} and the forming temperature is 673 K:

$$\sigma = A + B\varepsilon^n. \quad \text{(Eq 5)}$$

Taking the logarithm of both sides of Eq 5 gives (for the cases with $\sigma < A$):

$$\ln(A - \sigma) = \ln(-B) + n \ln \varepsilon. \quad \text{(Eq 6)}$$

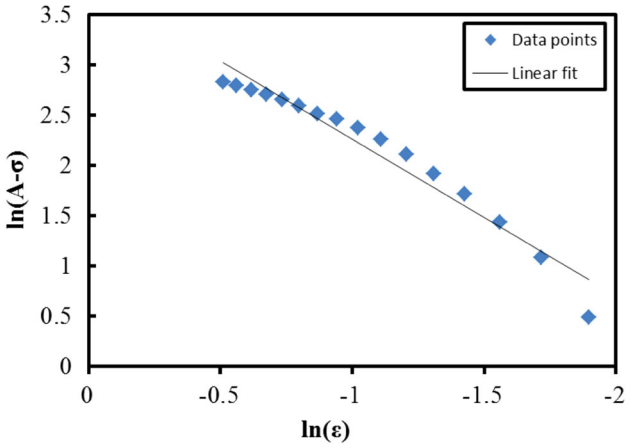

Fig. 4 The variation of ln (A − σ) vs. ln ε for the reference strain rate (0.001 s^{-1})

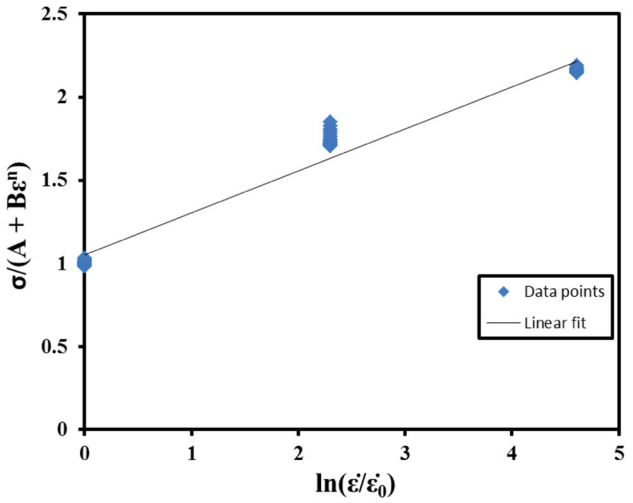

Fig. 5 Variation of $\sigma/(A + B\varepsilon^n)$ vs. $\ln(\dot{\varepsilon}/\dot{\varepsilon}_0)$

Then, substituting the values of the flow stress and corresponding strain values into the Eq 6 gives the relationship between ln $(A - \sigma)$ and ln ε, as is shown in Fig. 4. The value of n and B can be obtained from the slope and intercept of the fitting line in the ln $(A - \sigma)$ – ln ε plot; these are calculated to be 1.57 and −43.79 MPa, respectively. Where only the reference temperature is applied, Eq 4 can be simplified as

$$\frac{\sigma}{A + B\varepsilon^n} = 1 + C \ln(\dot{\varepsilon}/\dot{\varepsilon}_0). \quad \text{(Eq 7)}$$

The relationship between $\frac{\sigma}{A+B\varepsilon^n}$ and $\ln(\dot{\varepsilon}/\dot{\varepsilon}_0)$ has been plotted for a series of strains (0.03-0.6) in Fig. 5. Then, the material constant C (~0.25) has been calculated by linear fitting method. Here, only the average fitting line is shown in Fig. 5. Where only the reference strain rate is applied, Eq 4 can be expressed as is follows:

$$\frac{\sigma}{A + B\varepsilon^n} = 1 - T^{*p}. \quad \text{(Eq 8)}$$

Taking the logarithm of both sides of Eq 8 gives

$$\ln(1 - \sigma/\sigma_0 + B\varepsilon^n) = P \ln T^*. \quad \text{(Eq 9)}$$

Then, substituting the five different deformation temperatures (673, 773, 873, 973, and 1073 K) and the corresponding flow stress at different strains into Eq 9, the relationship between ln $[1 - \sigma/(\sigma_0 + B\varepsilon^n)]$ and ln T^* can be obtained (Fig. 6). Finally, p as the material constant is calculated to be 0.31 by linear fitting method. So, the original Johnson-Cook model for the experimental alloy can be summarized as

$$\sigma = \left(98.07 - 43.79\varepsilon^{1.57}\right)\left[1 + \frac{0.25 \ln(\dot{\varepsilon})}{\dot{\varepsilon}_0}\right](1 - T^{*0.31}). \quad \text{(Eq 10)}$$

The comparisons between the measured and predicted flow stresses through the original Johnson-Cook model are shown in Fig. 7. Obviously, the prediction can be accepted only under the reference temperature and reference strain rate.

3.1.2 Arrhenius-Type Constitutive Model. The strain-compensated Arrhenius-type equation (Eq 11) has been widely employed to describe the relationship between the strain rate, flow stress, and temperature, especially at high temperatures (Ref 34-36):

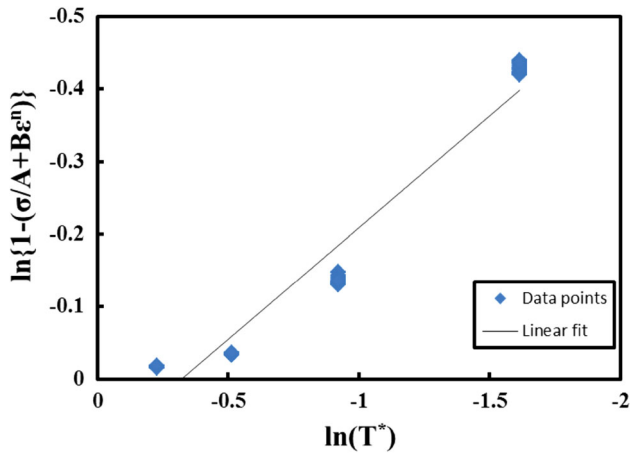

Fig. 6 The variation of ln $\{1 - (\sigma/A + B\varepsilon^n)\}$ vs. ln (T^*)

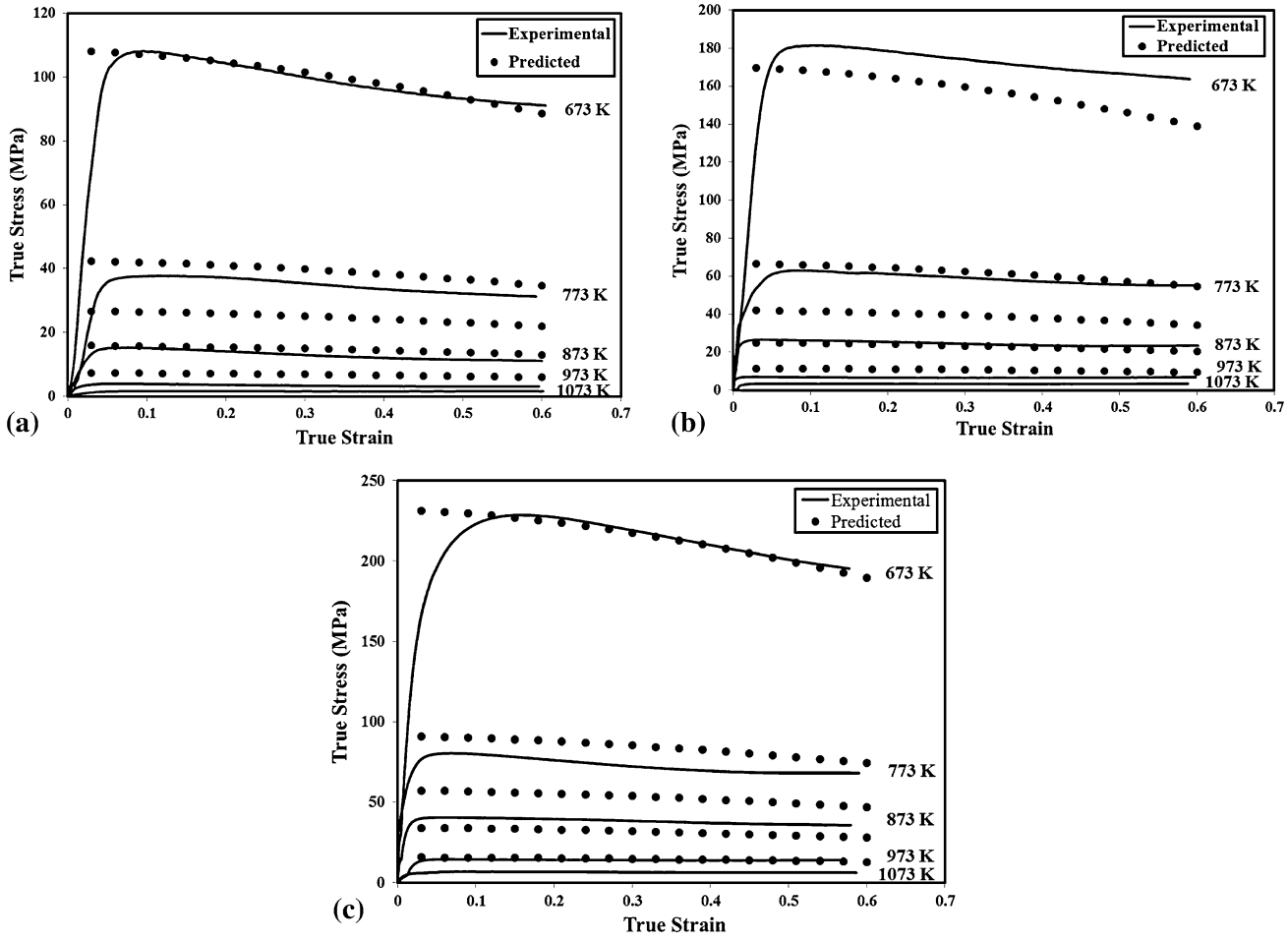

Fig. 7 Comparisons between measured and predicted flow stresses by original Johnson-Cook Model under the strain rates of: (a) 0.001 s^{-1}, (b) 0.01 s^{-1}, (c) 0.1 s^{-1}

$$\dot{\varepsilon} = AF(\sigma)\exp\left(-\frac{Q}{RT}\right), \quad \text{(Eq 11)}$$

where

$$F(\sigma) = \begin{cases} \sigma^{n_1}, & \alpha\sigma < 0.8 \\ \exp(\beta\sigma), & \alpha\sigma > 1.2 \\ [\sin h(\alpha\sigma)]^n & \text{for all } \sigma \end{cases},$$

where σ is the flow stress (MPa), $\dot{\varepsilon}$ is the strain rate (s^{-1}), Q is the effective activation energy of deformation (J/mol), R is the universal gas constant (8.314 J/(molK)), and A (s^{-1}), α (MPa^{-1}), n, n_1, and β are material constants, which are experimentally determined.

Furthermore, the effects of temperature and strain rate on the deformation behaviors can be characterized by Zener-Holloman parameter as is follows:

$$Z = \dot{\varepsilon}\exp\left(\frac{Q}{RT}\right). \quad \text{(Eq 12)}$$

In this study, the strain of 0.3 was taken as an example to introduce the solution procedures of the material constants. At a certain deformation temperature, for the low stress level ($\alpha\sigma < 0.8$) and high stress level ($\alpha\sigma > 1.2$), substituting the power law and exponential stress law of $[F(\sigma)]$ into Eq 8 gives the following equations:

$$\dot{\varepsilon} = B\sigma^{n_1}, \quad \text{(Eq 13)}$$

$$\dot{\varepsilon} = C\exp(\beta\sigma), \quad \text{(Eq 14)}$$

where B and C are the material constants. Taking the logarithm of both sides of Eq 13 and 14 to

$$\sigma = \frac{1}{\beta}\ln\dot{\varepsilon} - \frac{1}{\beta}\ln C, \quad \text{(Eq 15)}$$

$$\ln\sigma = \frac{1}{n_1}\ln\dot{\varepsilon} - \frac{1}{n_1}\ln B. \quad \text{(Eq 16)}$$

It is obvious that the relationship between flow stress and strain rate can be approximated by a group of parallel straight lines. As shown in Fig. 8(a) and (b), the value of n_1 and β can be obtained from the slope of the lines in the $\ln\sigma - \ln\dot{\varepsilon}$ and $\sigma - \ln\dot{\varepsilon}$ plots, respectively. Since the slopes of the lines are approximately the same, only the mean slope value is calculated; this gives the corresponding value of $\alpha = \beta/n_1$. For all the stress level (including low and high stress levels), Eq 11 can be written as

$$\dot{\varepsilon} = A[\sin h(\alpha\sigma)]^n \exp\left(-\frac{Q}{RT}\right). \quad \text{(Eq 17)}$$

Taking the logarithm from both sides of Eq 17 and rearranging them would yield to the following equation:

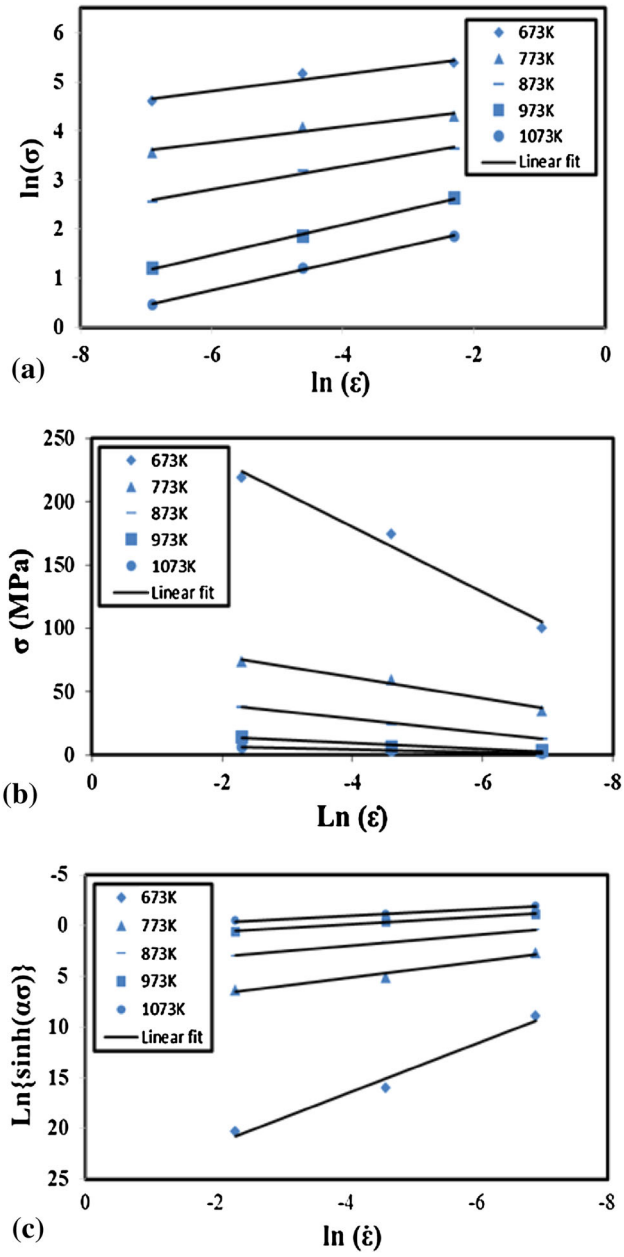

Fig. 8 The variation between: (a) $\ln\sigma - \ln\dot{\varepsilon}$; (b) $\sigma - \ln\dot{\varepsilon}$; (c) $\ln[\sin h(\alpha\sigma)] - \ln\dot{\varepsilon}$; (d) $\ln[\sin h(\alpha\sigma)] - 100/T$

$$\ln[\sin h(\alpha\sigma)] = \frac{\ln\dot{\varepsilon}}{n} + \frac{Q}{nRT} - \frac{\ln A}{n}. \quad \text{(Eq 18)}$$

By substituting the values of the strain rate and flow stress for the true strain of 0.3 at all the deformation temperatures into Eq 18, the $\ln[\sin h(\alpha\sigma)]$- $\ln\dot{\varepsilon}$ relationship and the n value can be obtained (Fig. 8c). Then constant A is also calculated from the intercept of $\ln[\sin h(\alpha\sigma)]$ versus $\ln\dot{\varepsilon}$ plot. For a particular strain rate, the Q-value can be also derived from the mean slope of $\ln[\sin h(\alpha\sigma)] - 1000/T$ plot (Fig. 9) through the following equation:

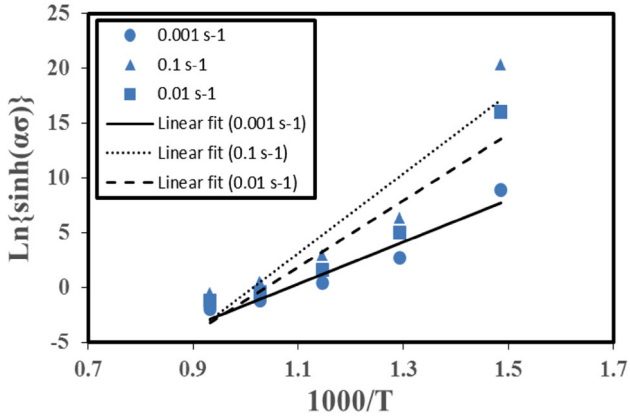

Fig. 9 The variation between $\ln[\sin h(\alpha\sigma)]$ vs. 1000/T

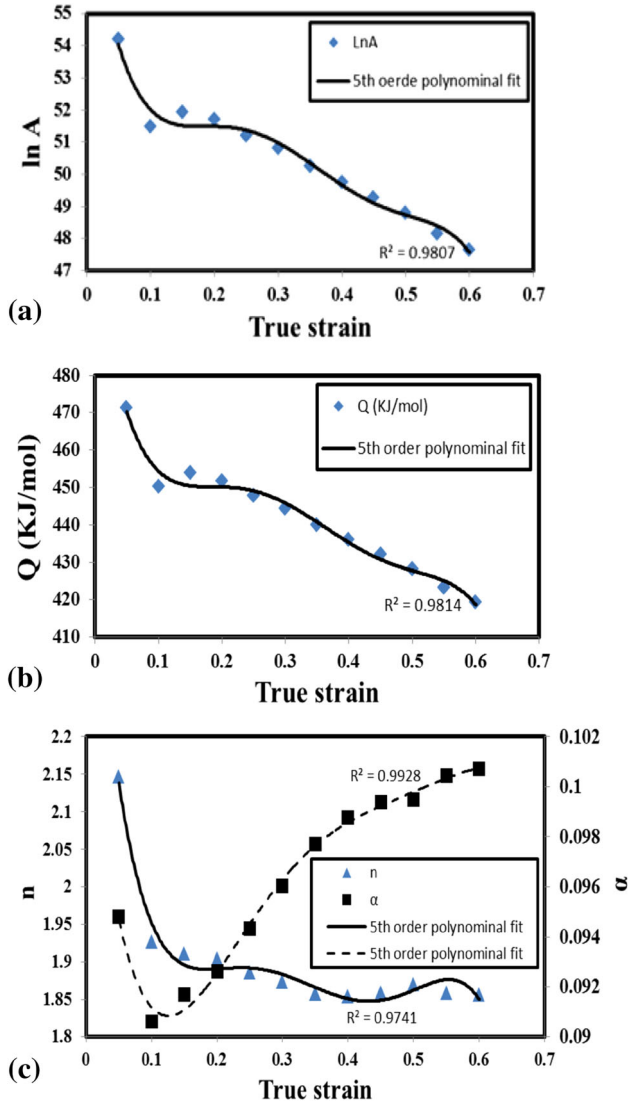

Fig. 10 The variation of (a) $\ln A$; (b) Q; (c) n and α with true strain

$$Q = 1000Rn\left[d\{\ln\sin h(\alpha\sigma)\}/d\left(\frac{100}{T}\right)\right]. \quad \text{(Eq 19)}$$

It is worth to note that the effect of imposed strain on the flow stress is significant; especially at the initial stage of deformation process thereby the strain effect should be taken into account. Accordingly, a method of compensation of strain (Ref 14) was used to increase the accuracy of the prediction where the material constants were evaluated under different strains, and were employed to fit into the polynomial functions of strain. A fifth order polynomial, as is shown in Eq. 20, was found to represent the influence of strain on material constants with a very good correlation and generalization (Fig. 10). The corresponding coefficients of the polynomial functions are given in Table 2.

Table 2 Coefficients of the polynomial for α, *n*, *Q* and ln *A*

A	*n*	*Q*	ln *A*
$a_0 = 2.5798$	$N_0 = 0.104$	$Q_0 = 510.54$	$A_0 = 59.223$
$a_1 = -12.467$	$N_1 = -0.2652$	$Q_1 = 1166.6$	$A_1 = -149.72$
$a_2 = 85.595$	$N_2 = 1.8209$	$Q_2 = 8507.4$	$A_2 = +1091.5$
$a_3 = -276.45$	$N_3 = -5.0723$	$Q_3 = -28690$	$A_3 = -3674.2$
$a_4 = 417.31$	$N_4 = 6.502$	$Q_4 = 43763$	$A_4 = 5598.8$
$a_5 = -237.05$	$N_5 = -3.1726$	$Q_5 = -24812$	$A_5 = -3173.2$

$$\begin{cases} \alpha = a_0 + a_1\varepsilon + a_2\varepsilon^2 + a_3\varepsilon^3 + a_4\varepsilon^4 + a_5\varepsilon^5 \\ n = N_0 + N_1\varepsilon + N_2\varepsilon^2 + N_3\varepsilon^3 + N_4\varepsilon^4 + N_5\varepsilon^5 \\ Q = Q_0 + Q_1\varepsilon + Q_2\varepsilon^2 + Q_3\varepsilon^3 + Q_4\varepsilon^4 + Q_5\varepsilon^5 \\ \ln A = A_0 + A_1\varepsilon + A_2\varepsilon^2 + A_3\varepsilon^3 + A_4\varepsilon^4 + A_5\varepsilon^5 \end{cases}. \quad \text{(Eq 20)}$$

After the material constants are evaluated, the flow stress for a particular strain can be predicted. Finally, according to the definition of the hyperbolic law, the flow stress can be written as a function of the Zener-Hollomon parameter:

$$\sigma = \frac{1}{\alpha}\ln\left\{\left(\frac{Z}{A}\right)^{\frac{1}{n}} + \left[\left(\frac{Z}{A}\right)^{\frac{2}{n}} + 1\right]^{\frac{1}{2}}\right\}. \quad \text{(Eq 21)}$$

The comparison between the experimental and predicted data from strain-compensated Arrhenius-type constitutive equation for various processing conditions is shown in Fig. 11. As is seen the predicted flow stresses are completely different with the experimental results in the entire processing domain. The following results have been seen in prediction of flow stress of Aermet100 steel (Ref 24).

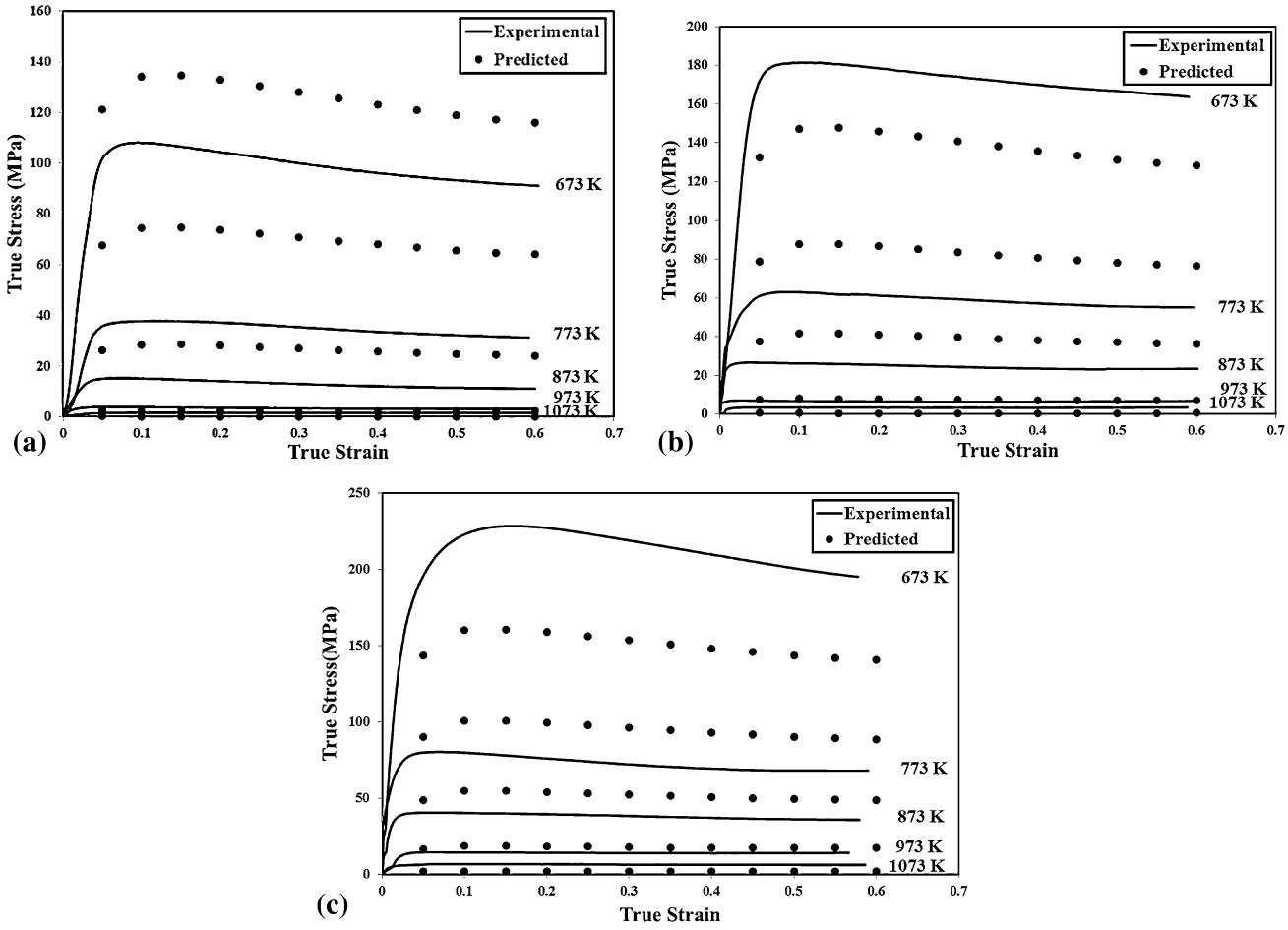

Fig. 11 Comparison between the experimental and predicted flow stresses by strain-compensated Arrhenius-type equation under the strain rate of (a) 0.001 s^{-1}, (b) 0.01 s^{-1}, (c) 0.1 s^{-1}

3.1.3 Modified Zerilli-Armstrong Model. In order to investigate the capability of physically based constitutive models, the modified Zerilli-Armstrong model for predicting the high temperature flow behavior has been employed. The modified equation can be represented as is follows:

$$\sigma = (C_1 + C_2\varepsilon^n)\exp[-(C_3 + C_4\varepsilon)T^* + (C_5 + C_6T^*)\ln\dot{\varepsilon}^*], \quad \text{(Eq 22)}$$

where σ is the flow stress, ε is the equivalent plastic strain, $\dot{\varepsilon}^* = \dot{\varepsilon}/\dot{\varepsilon}_0$ is the dimensionless strain rate with $\dot{\varepsilon}$ being the strain rate and $\dot{\varepsilon}_0$ the reference strain rate, $T^* = (T - T_{ref})$ with T and T_{ref} being the current and reference temperatures. C1, C2, C3, C4, C5, C6, n are the materials' constants. Similar to Johnson-Cook model, the reference temperature and the reference strain rate are taken to be 673 K and 0.001 s^{-1}, respectively. Where the reference strain rate is employed ($\dot{\varepsilon}^* = 1$):

$$\sigma = (C_1 + C_2)\exp[-(C_3 + C_4\varepsilon)T^*]. \quad \text{(Eq 23)}$$

Then, taking natural logarithm of both sides results in the following equation:

$$\ln\sigma = \ln(C_1 + C_2\varepsilon^n) - (C_3 + C_4\varepsilon)T^*. \quad \text{(Eq 24)}$$

Substituting the experimental flow stress data at $\dot{\varepsilon}^* = 1$ into Eq. 24, the relationship between ln σ and T^* is obtained, as is shown in Fig. 12. Then, the values of ln $(C_1 + C_2\varepsilon^n)$ and $-(C_3 + C_4\varepsilon)$ can be calculated.

$$I_1 = \ln(C_1 + C_2\varepsilon^n). \quad \text{(Eq 25)}$$

Rearranging the above equation yields

$$\ln(\exp I_1 - C_1) = \ln C_2 + n\ln\varepsilon. \quad \text{(Eq 26)}$$

Here, C_1 is the yield stress determined from the true stress-strain curve at reference temperature and strain rate. Substituting C_1 into Eq. 26, the relationship between ln $(\exp I_1 - C_1)$and ln ε is obtained (Fig. 13). Then, C_2 and n can be calculated from the intercept and slope of the plotted trend line. In the same way, the slope of the line represented by Eq. 23 can be written as

$$S_1 = -(C_3 + C_4\varepsilon). \quad \text{(Eq 27)}$$

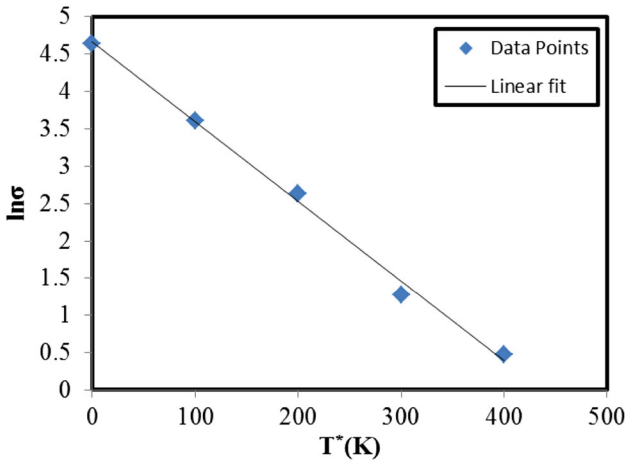

Fig. 12 The variation of ln σ vs. T^* for the strain of 0.21 at reference strain rate

Figure 14 shows the relationship between S_1 and ε, where $-C_3$ and $-C_4$ constants can be obtained through the corresponding intercept and the slope, respectively. By taking natural logarithm of Eq. 22, the following expression could be derived:

$$\ln\sigma = \ln(C_1 + C_2\varepsilon^n) - (C_3 + C_4\varepsilon)T^* + (C_5 + C_6T^*)\ln\dot{\varepsilon}^*. \quad \text{(Eq 28)}$$

The ln σ versus $\ln\dot{\varepsilon}^*$ plot gives the value of $(C_5 + C_6T^*)$ as the slope of plotted line. For different applied temperatures, different values of S_2 are obtained at a specific strain, and the slope can be represented as is follows:

$$S_2 = C_5 + C_6T^*. \quad \text{(Eq 29)}$$

Therefore, the relationship between S_2 versus T^* can be obtained (Fig. 15), where the value of C_5 and C_6 constants are calculated from the intercept and slope of the corresponding trend line, respectively. Finally, giving all of the material constants (Table 3), the developed constitutive equation based on modified Zerilli-Armstrong model is represented as is follows:

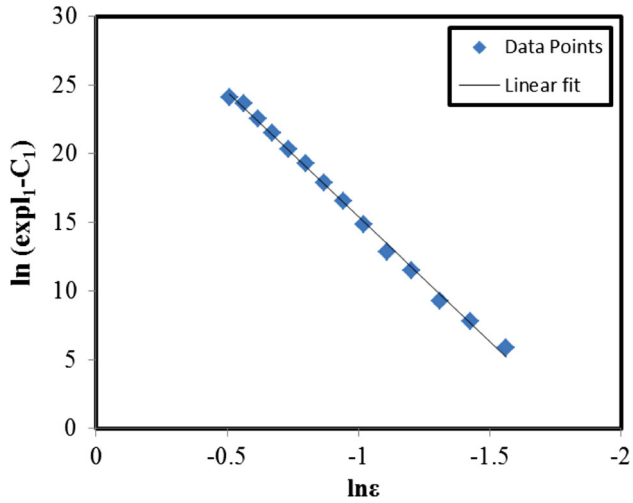

Fig. 13 The variation between $\ln(\exp I_1 - C_1)$ and ln ε

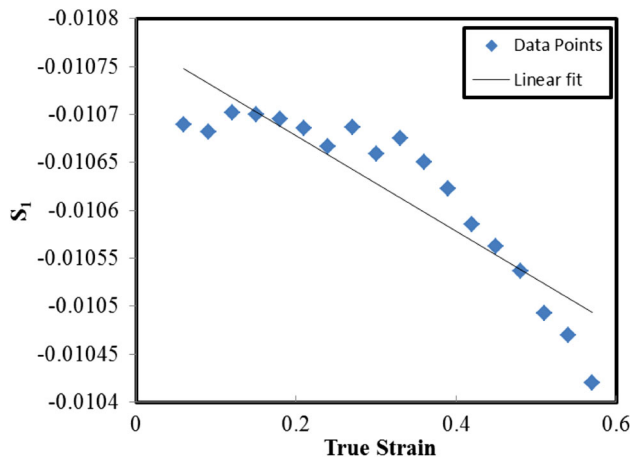

Fig. 14 The variation of S_1 with true strain

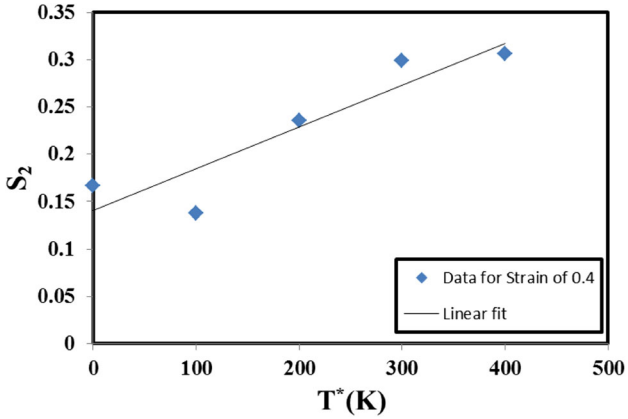

Fig. 15 The variation S_2 with T^*

$$\sigma = \left(98.07 - 23.63\varepsilon^{0.64}\right)\exp[-(0.0104 + 0.0002\varepsilon)T^* + (0.1407 + 0.00044T^*)\ln\dot{\varepsilon}^*]. \quad \text{(Eq 30)}$$

The flow stress data have been predicted accordingly for various thermomechanical processing conditions. As is observed in Fig. 16, the comparison between the experimental data and calculated ones indicates the high capability of modified Zerilli-Armstrong model for different processing conditions to predict the high temperature flow behavior of the experimental materials.

3.1.4 Verification of Developed Constitutive Models. As was shown, the original Johnson-Cook model can represent the high temperature flow behaviors of the experimental alloy only at the reference strain rate and temperature.

Table 3 Parameters for the modified Zerilli-Armstrong model to predict the high temperature flow stress of leaded duplex brass

Parameter	C1 (MPa)	C2 (MPa)	C3	C4	C5	C6	*n*
Value	98.07	−23.63	0.01065	0.00021	0.14077	0.00044	0.64

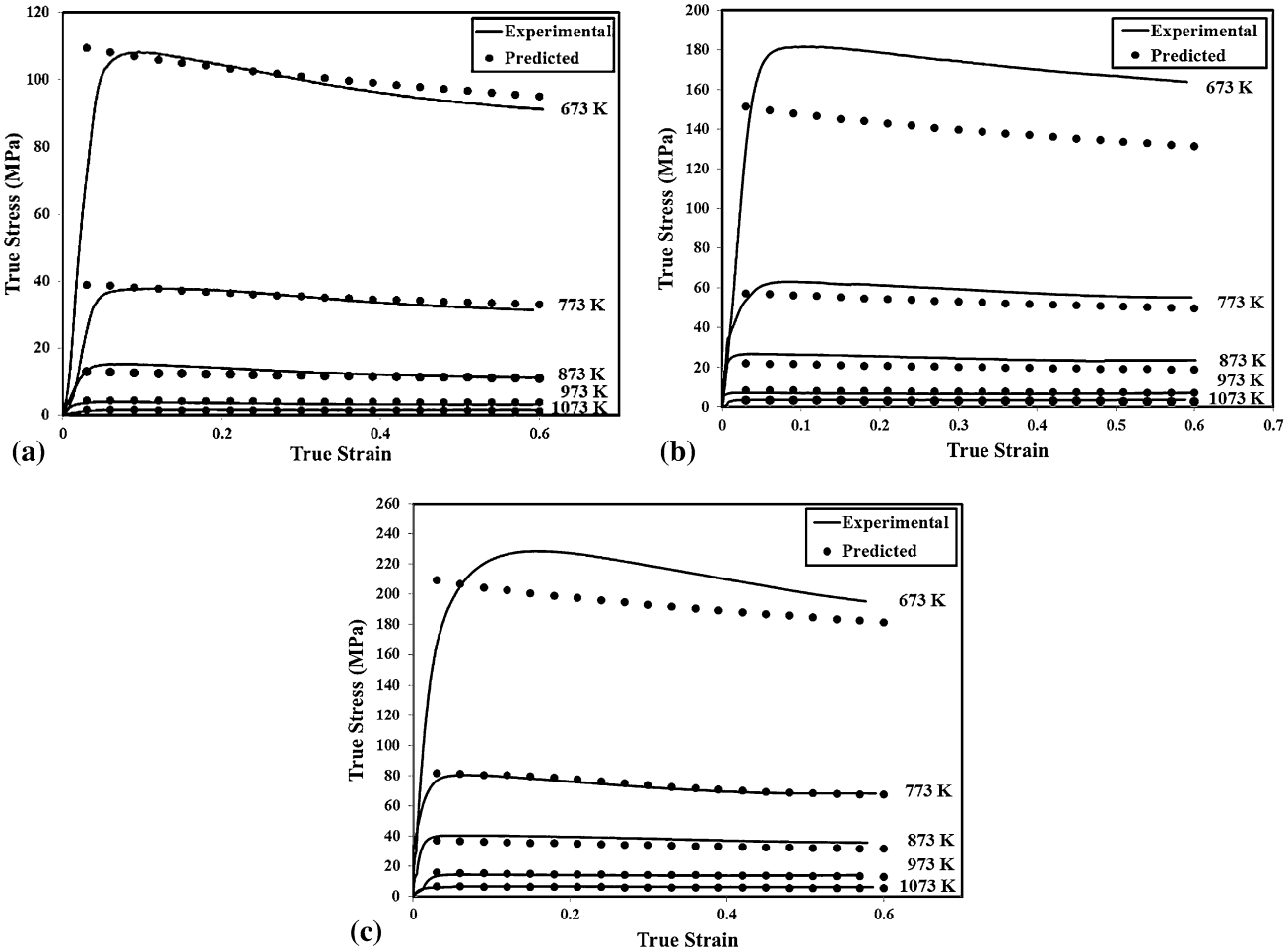

Fig. 16 Comparison between the experimental and predicted flow stresses utilizing the modified Zerilli Armstrong constitutive equation under the strain rate of: (a) 0.001 s^{-1}, (b) 0.01 s^{-1}, (c) 0.1 s^{-1}

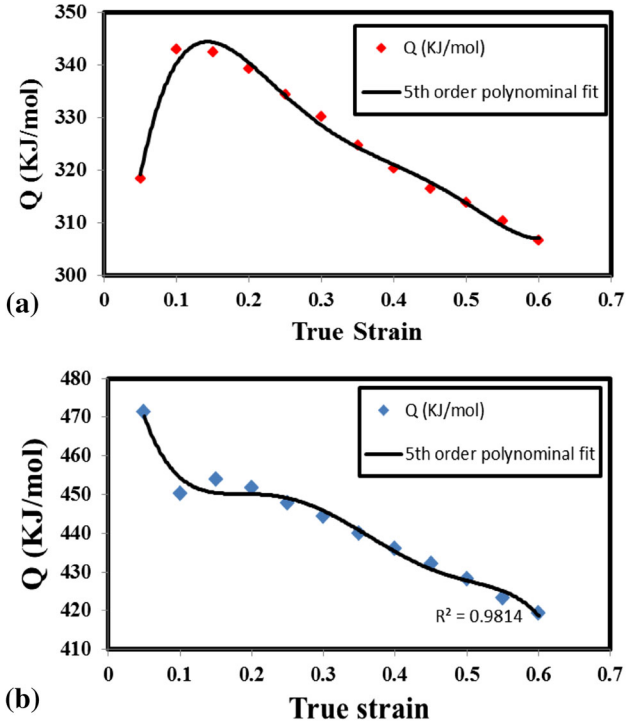

Fig. 17 The calculated activation energy (Q-value) in different test temperature ranges of: (a) 673-1073 K; (b) 773-1073 K

Apparently, where the differences of the applied strain rate and temperature are increased compared to the reference ones, the accuracy of the prediction decreases. The significant deviation in prediction is attributed to the fact that the original Johnson-Cook model assumes the thermal softening, strain-rate hardening, and strain hardening as three independent phenomena which can be isolated from each other. However, the coupled effects of temperatures, strain rates, and imposed strain should be considered on the flow stress behavior of the alloy.

The other phenomenological constitutive model (Arrhenius-type) cannot accurately predict the flow stress behavior of the material over the wide ranges of temperature and strain rate. As a matter of fact, the accuracy of Arrhenius-type constitutive model is strongly dependent on the Q-value which changes significantly through limiting the test temperature range. In this regard, the activation energy values have been recalculated at different temperature range and plotted versus strain rate in Fig. 17. These two temperature ranges (673-1073 K and 773-1073 K) have been adopted considering the fact that the flow stress level would be dramatically decreased by increasing the test temperature from 673 to 773 K (refer to Fig. 2). Evidently, this decrease in the stress level represents the changes in operated deformation mechanism, which directly determine the activation energy over the investigated temperature range. As is observed in Fig. 17, limiting the temperature range leads to a different and lower Q-value, which positively influences the accuracy of the proposed model. This is well rationalized

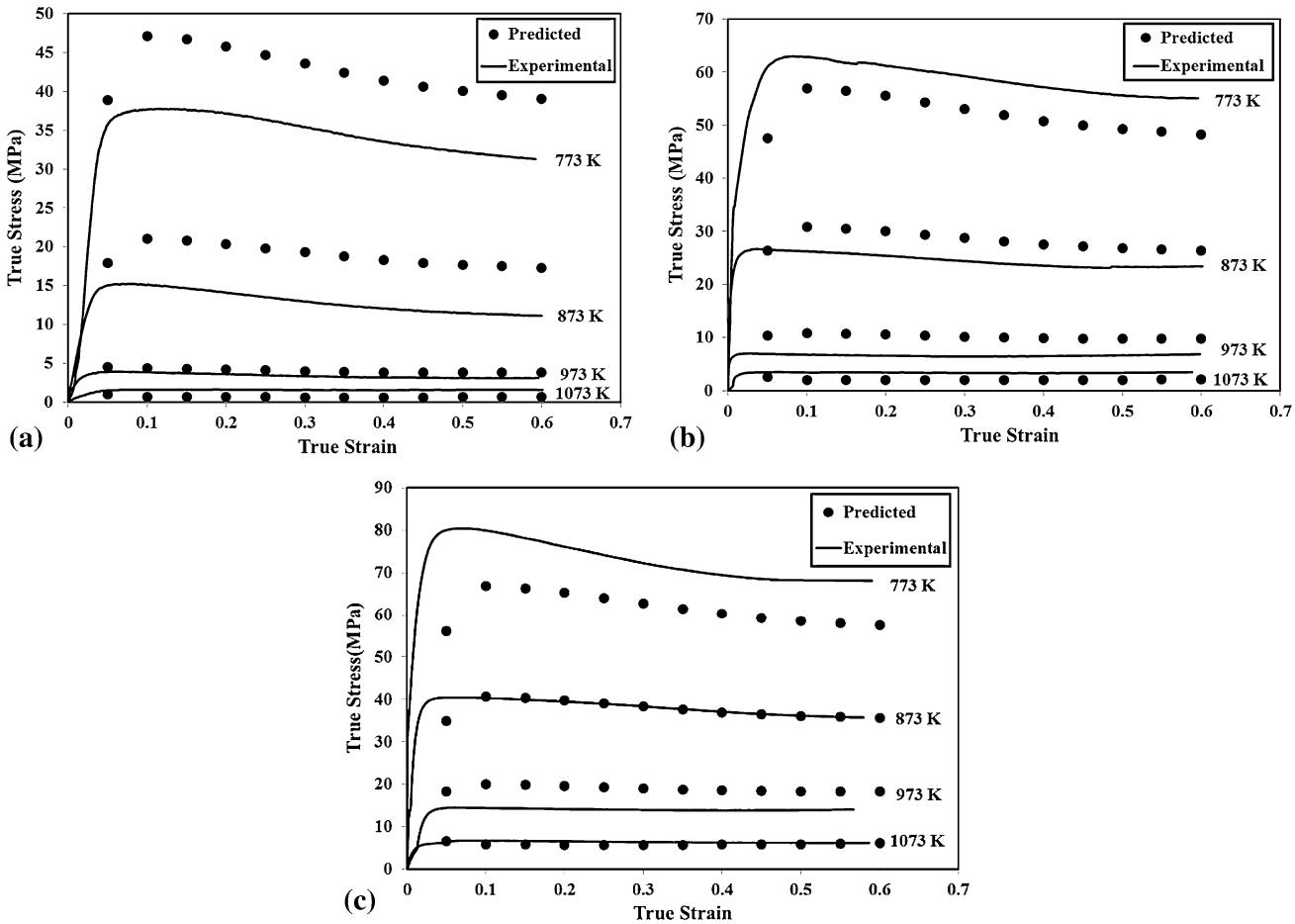

Fig. 18 Comparison between the experimental and predicted flow stress applying strain-compensated Arrhenius-type equation under the strain rate of (a) 0.001 s^{-1}, (b) 0.01 s^{-1}, (c) 0.1 s^{-1} in the temperature range of 773-1073 K

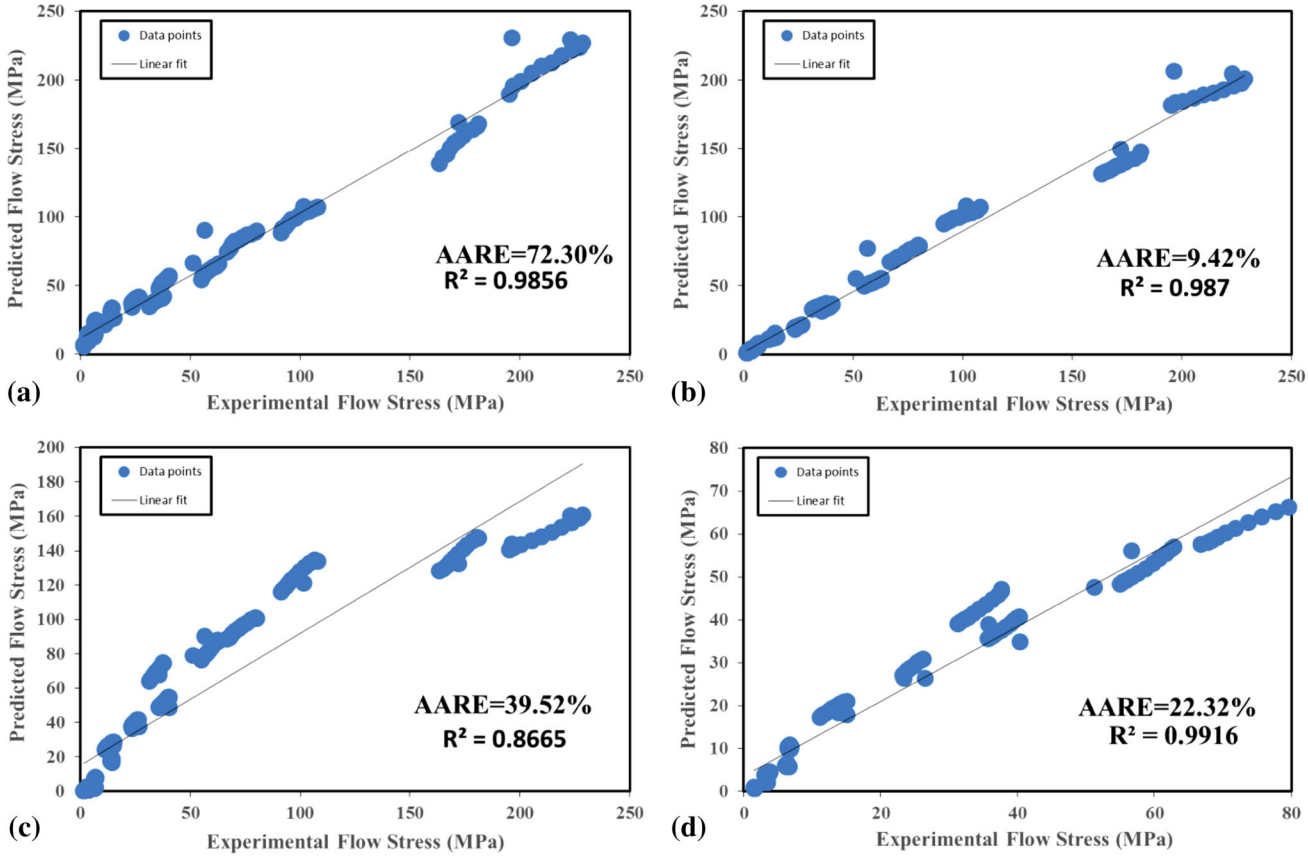

Fig. 19 Correlation between the experimental and predicted flow stress values from (a) the original Johnson-Cook model; (b) the modified Zerilli-Armstrong model; (c) the Arrhenius-type model in temperature range of 673-1073 K; (d) the Arrhenius-type model in temperature range of 773-1073 K

comparing to the prediction, which have been carried out at different temperature range (Fig. 18 and 11). Thus, there is a great debate around decision making through Arrhenius constitutive model in a wide temperature range, in which the deformation mechanisms changes significantly. On the contrary, the modified Zerilli-Armstrong model seems to be capable to overcome these shortcomings, because it properly considers the physical characteristics including dislocation dynamics and thermal activation to develop the materials constants. It should be considered that in developing Zerilli-Armstrong model to predict the flow stress, the reference strain rate and temperature have been employed (here the reference strain rate is 0.001 s^{-1} and the reference temperature is 673 K). Apparently, the modified Zerilli-Armstrong equation is sensitive to these reference conditions, and deviates from the experimental stress values where the severe deformation conditions are applied. This deviation has been also reported in previous researches (Ref 23, 26). However, the capability of this model is in good agreement with previous reported data in the case of modified 9Cr-1Mo steel (Ref 23) and T24 steel (Ref 25).

The accuracy of the mentioned models is also verified via employing standard statistical parameters such as AARE and correlation coefficient. AARE is an unbiased statistical parameter for measuring the predictability of a model/equation, and is calculated through a term-by-term comparison of the relative error (Ref 37). The correlation coefficient (R) provides information on the strength of linear relationship between the experimental and the predicted values. They can be expressed as

$$\mathrm{AARE}(\%) = \frac{1}{N}\sum_{i=1}^{N}\left|\frac{E_i - P_i}{E_i}\right| \times 100, \qquad \text{(Eq 31)}$$

$$R = \frac{\sum_{i=1}^{N}(E_i - \bar{E})(P_i - \bar{P})}{\sqrt{\sum_{i=1}^{N}(E_i - \bar{E})^2 \sum_{i=1}^{N}(P_i - \bar{P})^2}}, \qquad \text{(Eq 32)}$$

where E_i is the experimental data and P_i is the predicted value obtained from the constitutive equation. $\bar{E}$ and $\bar{P}$ are the mean values of E and P, respectively. N is the total number of data employed in the investigation. Figure 19 shows the plots of experimental values and predicted values predicted by the three developed models, respectively. The AARE of the modified Zerilli-Armstrong, original Johnson-Cook, and Arrhenius-type models are calculated to be 9.42, 72.30, and 39.52%, respectively. This also indicates that the modified Zerilli-Armstrong model has the best correlation between the predicted results and experimental ones in comparison to the other phenomenological models.

4. Conclusions

A comparative study has been made on the ability of the phenomenological (original Johnson-Cook and Arrhenius-type) and the physical (modified Zerilli-Armstrong) constitutive models, to describe the elevated temperature flow behavior of

leaded duplex brass in the temperature range of 673-1073 K with the strain rate of 0.001-0.1 s^{-1}. The results indicate that the Original Johnson-Cook model may not consider the coupled effects of temperatures, strain rates, and imposed strain; the flow stress predictions would be only accurate at reference temperature and strain rate. The Arrhenius-type constitutive inherits inaccuracy of predictions due to the inability of the equation in acquiring the precise activation energy (Q-value) in a wide processing domain.However, the modified Zerilli-Armstrong constitutive equation could predict the flow stress more accurately and could be considered as the best model for predicting the high temperature flow stress behavior of leaded duplex brass. These findings are also verified through calculating the related statistical parameters, where AAREs for the original Johnson-Cook, Arrhenius-type, and modified Zerilli-Armstrong models are 72.30, 39.52, and 9.42% respectively.

References

1. C.R. Brooks, *Heat Treatment, Structure, and Properties of Nonferrous Alloys*, American Society for Metals, Metals Park, 1982
2. D. Padmavardhani and Y.V.R. Prasad, Characterization of Hot Deformation Behavior of Brasses Using Processing Maps: Part I. α Brass, *Met. Trans.*, 1991, **V22A**, p 2993
3. N. Haghdadi, A. Zarei-Hanzaki, and H.R. Abedi, The Flow Behavior Modeling of Cast A356 Aluminum Alloy at Elevated Temperatures Considering the Effect of Strain, *Mater. Sci. Eng. A*, 2012, **535**, p 252–257
4. N.S. Reddy, High Temperature Deformation Behavior of Ti-6Al-4V Alloy with an Equiaxed Microstructure: A Neural Networks Analysis, *Met. Mater. Int.*, 2008, **14**, p 213
5. M. Abo-Elkhier, Modeling of High-Temperature Deformation of Commercial Pure Aluminum (1050), *J. Mater. Eng. Perform.*, 2004, **13**, p 241
6. Y.C. Lin and X.-M. Chen, A Critical Review of Experimental Results and Constitutive Descriptions for Metals and Alloys in Hot Working, *Mater. Des.*, 2011, **32**, p 1733
7. R. Bhattacharya, Y.J. Lan, B.P. Wynne, B. Davis, and W.M. Rainforth, Constitutive Equations of Flow Stress of Magnesium AZ31 Under Dynamically Recrystallizing Conditions, *J. Mater. Process. Technol.*, 2014, **214**, p 1408
8. G.R Johnson, W.H. Cook, A Constitutive Model and Data for Metals Subjected to Large Strains, High Strain Rates and High Temperatures, *Proceedings of the 7th International Symposium on Ballistics,* vol. 21, International Ballistics Committee, The Hague, Netherlands, 1983, p 541-547
9. R. Liang and A.S. Khan, A Critical Review of Experimental Results and Constitutive Models for BCC and FCC Metals Over a Wide Range of Strain Rates and Temperatures, *Int. J. Plast*, 1999, **15**, p 963
10. Y.C. Lin, Q.F. Li, Y.C. Xia, and L.T. Li, A Phenomenological Constitutive Model for High Temperature Flow Stress Prediction of Al-Cu-Mg Alloy, *Mater. Sci. Eng. A*, 2012, **534**, p 654–662
11. C.M. Sellars and W.J. McTegart, On the Mechanism of Hot Deformation, *Acta Metall.*, 1966, **14**, p 1136
12. F.A. Slooff, J. Zhou, J. Duszczyk, and L. Katgerman, Constitutive Analysis of Wrought Magnesium Alloy Mg-Al4-Zn1, *Scr. Mater.*, 2007, **57**, p 759
13. Z. Zeng, S. Jonsson, and Y. Zhang, Constitutive Equations for Pure Titanium at Elevated Temperatures, *Mater. Sci. Eng. A*, 2009, **505**, p 116
14. Y.C. Lin, M.-S. Chen, and J. Zhong, Effect of Temperature and Strain Rate on the Compressive Deformation Behavior of 42CrMo Steel, *J. Mater. Process. Technol.*, 2008, **205**, p 308
15. S. Mandal, V. Rakesh, P.V. Sivaprasad, S. Venugopal, and K.V. Kasiviswanathan, Constitutive Equations to Predict High Temperature Flow Stress in a Ti-Modified Austenitic Stainless Steel, *Mater. Sci. Eng. A*, 2009, **500**, p 114
16. A. Etaati, K. Dehghani, G.R. Ebrahimi, and H. Wang, Predicting the Flow Stress Behavior of Ni-42.5Ti-3Cu During Hot Deformation Using Constitutive Equations, *Met. Mater. Int.*, 2013, **19**, p 5–9
17. R.K. Oruganti and K.P. Rao, Flow Stress Modeling for Copper under Changing Process Conditions, *Met. Mater.*, 1998, **4**, p 472–476
18. G. Ji, G. Yang, L. Li, and Q. Li, Modeling Constitutive Relationship of Cu-0.4 Mg Alloy During Hot Deformation, *J. Mater. Eng. Perform.*, 2014, **23**, p 1770
19. D. Samantaray, S. Mandal, U. Borah, A.K. Bhaduri, and P.V. Sivaprasad, A Thermo-viscoplastic Constitutive Model to Predict Elevated-Temperature Flow Behaviour in a Titanium-Modified Austenitic Stainless Steel, *Mater. Sci. Eng. A*, 2009, **526**, p 1–6
20. J. Li, F. Li, J. Cai, R. Wang, Z. Yuan, and G. Ji, Comparative Investigation on the Modified Zerilli-Armstrong Model and Arrhenius-Type Model to Predict the Elevated-Temperature Flow Behaviour of 7050 Aluminium Alloy, *Comput. Mater. Sci.*, 2013, **71**, p 56
21. F.J. Zerilli and R.W. Armstrong, Dislocation Mechanics Based Constitutive Relations for Material Dynamics Calculations, *J. Appl. Phys.*, 1987, **61**, p 1816
22. A. He, G. Xie, H. Zhang, and X. Wang, A Modified Zerilli-Armstrong Constitutive Model to Predict Hot Deformation Behavior of 20CrMo Alloy Steel, *Mater. Des.*, 2014, **56**, p 122
23. D. Samantaray, S. Mandal, and A.K. Bhaduri, A Comparative Study on Johnson Cook, Modified Zerilli-Armstrong and Arrhenius-Type Constitutive Models to Predict Elevated Temperature Flow Behaviour in Modified 9Cr-1Mo Steel, *Comput. Mater. Sci.*, 2009, **47**, p 568–576
24. G. Ji, F. Li, Q. Li, H. Li, and Z. Li, A Comparative Study on Arrhenius-Type Constitutive Model and Artificial Neural Network Model to Predict High-Temperature Deformation Behaviour in Aermet100 Steel, *Mater. Sci. Eng. A*, 2011, **528**, p 4774
25. H.-Y. Li, X.-F. Wang, D.-D. Wei, J.-D. Hu, and Y.-H. Li, A Comparative Study on Modified Zerilli-Armstrong, Arrhenius-Type and Artificial Neural Network Models to Predict High-Temperature Deformation Behavior in T24 Steel, *Mater. Sci. Eng. A*, 2012, **536**, p 216
26. Y.C. Lin and X.-M. Chen, A Combined Johnson-Cook and Zerilli-Armstrong Model for Hot Compressed Typical High-Strength Alloy Steel, *Comput. Mater. Sci.*, 2010, **49**, p 628
27. Y.C. Lin, Y.-C. Xia, X.-M. Chen, and M.-S. Chen, Constitutive Descriptions for Hot Compressed 2124-T851 Aluminum Alloy Over a Wide Range of Temperature and Strain Rate, *Comput. Mater. Sci.*, 2010, **50**, p 227
28. R. Ebrahimi and A. Najafizadeh, A New Method for Evaluation of Friction in Bulk Metal Forming, *J. Mater. Process. Technol.*, 2004, **152**, p 136–143
29. H. Monajati, M. Jahazi, S. Yue, and A.K. Taheri, Deformation Characteristics of Isothermally Forged UDIMET 720, *Nickel-Base Superalloy*, 2005, **36**, p 895
30. Y.P. Li, E. Onodera, H. Matsumoto, and A. Chiba, Correcting the Stress-Strain Curve in Hot Compression Process to High Strain Level, *Metall. Mater. Trans. A*, 2009, **40**, p 982
31. E. Farghadany, A. Zarei-Hanzaki, H.R. Abedi, D. Dietrich, and T. Lampke, The Strain Accommodation in Ti-28Nb-12Ta-5Zr Alloy During Warm Deformation, *Mater. Sci. Eng. A*, 2014, **592**, p 57
32. H.R. Abedi, A. Zarei-Hanzaki, S.M. Fatemi-Varzaneh, and A.A. Roostaei, The Semi-solid Tensile Deformation Behavior of Wrought AZ31 Magnesium Alloy, *Mater. Des.*, 2010, **31**, p 4386
33. D. Padmavardhani, Characterization of Hot Deformation Behavior of Brasses Using Processing Maps: Part II. β Brass and α/β Brass, *Metall. Trans. A*, 1991, **22**, p 2993
34. M.R. Rokni, A. Zarei-Hanzaki, A.A. Roostaei, and A. Abolhasani, Constitutive Base Analysis of a 7075 Aluminum Alloy During Hot Compression Testing, *Mater. Des.*, 2011, **32**, p 4955
35. A. Mirzaei, A. Zarei-Hanzaki, N. Haghdadi, and A. Marandi, Constitutive Description of High Temperature Flow Behavior of Sanicro-28 Super-Austenitic Stainless Steel, *Mater. Sci. Eng. A*, 2014, **589**, p 76
36. H. Yu, H. Yu, G. Min, S.S. Park, B.S. You, and Y.M. Kim, Strain-Dependent Constitutive Analysis of Hot Deformation and Hot Workability of T4-Treated ZK60 Magnesium Alloy, *Met. Mater. Int.*, 2013, **19**, p 651
37. X. Ma, W. Zeng, F. Tian, Y. Sun, and Y. Zhou, Modeling Constitutive Relationship of BT25 Titanium Alloy During Hot Deformation by Artificial Neural Network, *J. Mater. Eng. Perform.*, 2011, **21**, p 1591